Ocean Dynamics (2014) 64:347–360
DOI 10.1007/s10236-014-0699-4

# Sea surface temperature anomalies driven by oceanic local forcing in the Brazil-Malvinas Confluence

**Isabel Porto da Silveira · Luciano Ponzi Pezzi**

Received: 13 August 2013 / Accepted: 24 January 2014 / Published online: 11 February 2014


**Abstract** Sea surface temperature (SST) anomaly events in the Brazil-Malvinas Confluence (BMC) were investigated through wavelet analysis and numerical modeling. Wavelet analysis was applied to recognize the main spectral signals of SST anomaly events in the BMC and in the Drake Passage as a first attempt to link middle and high latitudes. The numerical modeling approach was used to clarify the local oceanic dynamics that drive these anomalies. Wavelet analysis pointed to the 8–12-year band as the most energetic band representing remote forcing between high to middle latitudes. Other frequencies observed in the BMC wavelet analysis indicate that part of its variability could also be forced by low-latitude events, such as El Niño. Numerical experiments carried out for the years of 1964 and 1992 (cold and warm El Niño-Southern Oscillation (ENSO) phases) revealed two distinct behaviors that produced negative and positive sea surface temperature anomalies on the BMC region. The first behavior is caused by northward cold flow, Río de la Plata runoff, and upwelling processes. The second behavior is driven by a southward excursion of the Brazil Current (BC) front, alterations in Río de la Plata discharge rates, and most likely by air-sea interactions. Both episodes are characterized by uncoupled behavior between the surface and deeper layers.

**Keywords** South Atlantic · Brazil-Malvinas Confluence · Ocean circulation · Sea surface temperature anomalies · Spectral analysis · Ocean model

Responsible Editor: Aida Alvera-Azcárate

I. P. da Silveira (✉) · L. P. Pezzi
National Institute for Space Research (INPE), SERE II, sala 12, Avenida dos Astronautas, 1758, 12227-010 São José dos Campos, São Paulo, Brazil
e-mail: isabel.silveira@cptec.inpe.br

L. P. Pezzi
e-mail: luciano.pezzi@cptec.inpe.br

I. P. da Silveira
Center for Weather Forecast and Climate Studies (CPTEC), Av. dos Astronautas, 1758, 12227-010 São José dos Campos, Brazil

L. P. Pezzi
Earth Observation General Coordination (OBT), Av. dos Astronautas, 1758, 12227-010 São José dos Campos, Brazil

## 1 Introduction

Sea surface temperature (SST) anomalies have been reported as among the most important signals for air-sea-coupled climate events because they can be used to obtain climate indexes (Trenberth 1997; Trenberth and Stepaniak 2001). Air-sea interactions mediated by changes in SST anomalies are well reported in the literature (Diaz et al. 1998; Pezzi and Cavalcanti 2001; Wainer and Venegas 2002), especially in tropical regions. As an example, El Niño events are popularized as being the "heating of the equatorial Pacific waters" that drive "dry/wet conditions" around the world. However, the role of SST anomalies in other regions of the world remains unclear, and how they form is also the subject of scientific discussion.

The atmospheric contribution to the formation and maintenance of these anomalies is related to positive feedback between SST anomalies and cloud cover at low levels, which is driven by increased in solar radiation (Klein et al. 1995). Zhang et al. (1998) suggested that feedback could generate a persistent signal from summer to winter seasons. Xie (2004) identified a positive correlation between SST and wind, where wind acts as a SST trapper and generator. Namias and Born (1974) were the first to note that SST trends reappear from one winter to the next in middle latitudes. These thermal

anomalies are incorporated by the seasonal thermocline during summer until the following fall, when the mixed layer is deeper and the SST anomalies are again exposed (Alexander and Penland 1996).

SST anomalies have been observed in the Southwestern Atlantic Ocean with some periodicity (e.g., Venegas et al. 1996; Diaz et al. 1998; Piola and Matano 2001; Lentini et al. 2001). Lentini et al. (2001) documented a total of 13 cold SST anomaly events and seven warm events in the western South Atlantic, based on a 13-year time series spanning from 1982 to 1994. The appearance and periodicity of these events are not completely understood. Some authors linked this variability to regional oceanic conditions characterized by the systems of fronts in the Brazil-Malvinas Confluence (BMC) at approximately 38°S (Matano et al. 1993; Garzoli and Giulivi 1994) and the intrusion of Río de la Plata discharge rates. The northward penetration from the Río de la Plata is evident year-round, reaching up to 32°S and 28°S during austral summer and winter, respectively (Piola et al. 2000). However, SST effects on the near-surface atmosphere could drive changes on climatological and interannual timescales (Tokinaga et al. 2005). At higher frequencies, the oceanic thermal contrast in this region is associated with (de)intensification or genesis of extra-tropical cyclones (Gan and Rao 1991; Hoskins and Hodges 2005). On smaller scales, the thermal contrast can contribute to marine atmospheric boundary layer (MABL) pressure variability and stability modifications, causing turbulent processes (Pezzi et al. 2005, 2009; Acevedo et al. 2010; de Camargo et al. 2013).

The BMC is formed through the convergence of the Brazil Current (BC) and the Malvinas Current (MC), which present contrasting characteristics. The BC is saltier and warmer than the MC, resulting in formation of an oceanic front. This intense temperature gradient is associated with salinity and density gradients at the surface and at depth. The BMC's vertical structure is also very complex and variable. During austral summer, the warmer and saltier tropical water carried by the BC is predominant (Möller et al. 2008). However, in the winter, the BC's influence drastically diminishes, decreasing the formation of South Atlantic central water (SACW) and increasing the influence of subantarctic shelf water (SASW) because of the northern penetration of the MC (Möller et al. 2008). Between the surface and a depth of 100 m, the temperature distribution of the BMC has fronts with distinct orientations (Conkright et al. 2002). This thermal uncoupling is typical of austral summer (Provost et al. 1996). When heat advection is observed, the water column presents three distinct layers because of BMC spatial-temporal variability: from the surface to 150 m, from 150 m to 400 m and from 400 m to the bottom (Bonatti and Rao 1999).

On the surface, the BC is reported to transport SACW southward and is characterized by temperatures between 10° and 23 °C and by salinities between 35 and 36 (Bianchi et al. 1993). The MC transports subantarctic water (SAAW) northward in the upper 500 m and features temperatures less than 10 °C and salinity lower than 34.3. The interaction between SACW and SAAW produces subtropical mode water (STMW) and subantarctic mode water (SAMW) as described by Maamaatuaiahutapu et al. (1992). The SAMW sinks at the BMC to form Antarctic intermediate water (AAIW), where isopycnals between 27.0 and 27.5 mark the transition between the SACW and the AAIW. The AAIW also receives an injection of water from the Benguela Current system (Garzoli and Gordon 1996). At intermediate depths, it flows equatorward (Cunningham and Barker 1996). At depths of approximately 800 to 1,000 m, the AAIW presents a salinity of 34.2 and a temperature range from 3.7 to 4.8 °C. Between 1,000 and 3,200 m, the circumpolar deep water (CDW) and the North Atlantic deep water (NADW) coexist, occupying a density range of 36.75 to 37.15 and flowing poleward (Bianchi et al. 1993 and the references therein). At the very bottom of the BMC zone, the Weddell Sea deep water flows westward (Cunningham and Barker 1996).

The BMC horizontal characterization is composed of a horizontal temperature gradient as high as 1 °C per 100 m (Gordon and Greengrove 1986). Möller et al. (2008) subdivided the MC waters into subantarctic water and subantarctic shelf water, whereas the tropical/subtropical water is composed of tropical water, subtropical shelf water, and SACW. subantarctic water, tropical water, and Río de la Plata water drive BMC seasonal variability through their local presence or absence. This influence can be observed through remote sensing (Olson et al. 1988; Goni and Wainer 2001; Saraceno et al. 2004). During austral summer, the BMC reaches its southernmost extent; during austral winter, it reaches its northernmost extent. This seasonal migration is the subject of debate. On the one hand, Matano et al. (1993) suggested that this process is driven by the annual cycle of wind stress curl and is dependent on the variability of the mass transported by the BMC currents. On the other hand, Garzoli and Giulivi (1994) did not find any correlation between the front position, the wind-forced pulses in the Antarctic circumpolar current, and the observed anomalous northward penetration of the MC. It was found that the variability in the location of the front results from the seasonal cycle of the winds in the South Atlantic. Through 9 years of radiometer analysis, Saraceno et al. (2004) observed that the fronts that present changes in the position and intensity at seasonal to interannual timescales are modulated by the bathymetry. These authors also refute the large seasonal north-south excursions of the Brazil Current front, although it pivots seasonally at approximately 39.5°S, 53.5°W, changing its orientation from N-S in winter to NW-SE in summer. However, the origins of MC seasonal variability in the BMC are related to regional and circumpolar wind fields, where the local forcing appears to respond to changes in the wind stress curl and in the remote forcing linked to the Drake Passage (Vivier et al.

2001). Witter and Gordon (1999) attributed the changes in sea level on a time scale of 2 to 3 years to meridional variations in the latitude of the confluence and to variations in the local distribution of eddy variability. Sea-level fields also indicate that this mode is linked to changes in the surface velocity of the MC (Witter and Gordon 1999).

Within this very complex BMC system, the main goal of this study is to clarify the dynamic processes that contribute to the formation of sea temperature anomalies in this region. This paper is outlined as follows. Section 2 presents the data, wavelet, and numerical modeling procedures. Time-energy variability analysis and SST dynamical analysis based on data and numerical simulations are presented in Section 3 of the results and discussion. The paper finishes with a section presenting our conclusions and suggestions for future studies.

## 2 Data and methods

### 2.1 Data and spatial analysis

As mentioned above, the study area is the Brazil-Malvinas Confluence (BMC), between 30°S to 45°S and 40°W to 60°W. The Drake Passage, extending from 55°S to 60°S and from 55°W to 75°W, was chosen as the second area for the present study. These areas were chosen in an attempt to find teleconnections between high and mid latitudes through the MC (Fig. 1). The MC injects relatively fresh and cold intermediate waters into the South Atlantic and contributes to water mass transformations in the Argentinean Basin (Garzoli and Matano 2011). The links between MC variability and atmospheric and oceanic circulation in the Southern Ocean are not well understood, although there is evidence that low-frequency variations in MC transport are connected to variations of Antarctic circumpolar current (ACC) transport in the Drake Passage and wind stress forcing in the Westerlies region (Vivier et al. 2001; Fetter and Matano 2008; Spadone and Provost 2009).

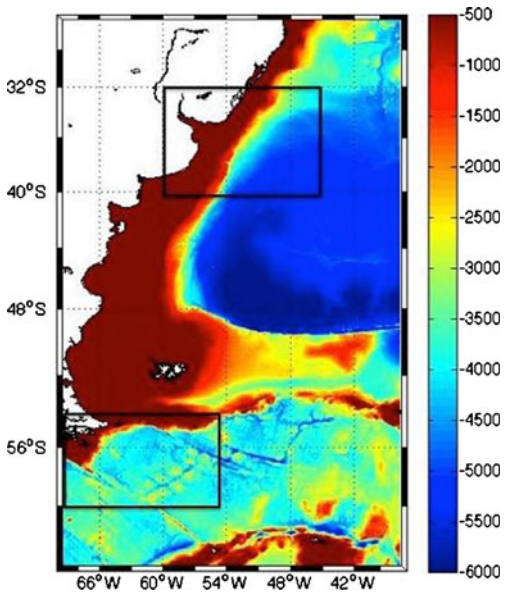


**Fig. 1** **a–d** The BMC study area is shown in the *upper rectangle*. The second area of interest is the Drake Passage in the *lower rectangle*. Bathymetry is shown in a *color gradient* (meters)

The BMC has been frequently studied using satellite remote sensing because of its thermal gradients and sea height anomalies (e.g., Souza et al 2006; Barré et al 2006; Chelton et al. 1990; Garcia et al. 2004; Legeckis and Gordon 1982; Olson et al. 1988). However, the present study is dedicated to elucidating the water column processes and the time variability in this region. In this context, the simple ocean data assimilation (SODA, Carton et al. 2000) reanalysis was used because of its long period of data and its facility in accessing water column data. SODA constructs datasets with observations of historical hydrographic profiles, supplemented by ship intake measurements, moored hydrographic observations, and remotely sensed SST assimilations. The reanalysis is a retrospective monthly analysis, covering the period from 1958 to 2001, provided on a grid with a horizontal resolution of 1° latitudinal by 1° longitudinal and 40 vertical levels with 10 m of vertical resolution in the upper 100 m and decreasing resolution at greater depths (Carton and Giese 2008). This dataset produces robust space-time investigations, such as those described by Katsumata and Masuda (2013), Lübbecke and McPhaden (2013), Zhu et al. (2012), and Corre et al. (2010). In this study, sea temperature, salinity, and wind stress components were used to obtain the BMC anomalies.

As a first approach, climatology and anomalies were evaluated from SODA reanalysis. Monthly climatology was calculated by taking the long-term monthly mean from the temporal series at all grid points. The anomalies were obtained through subtraction of the climatology from the original data. In this manner, 12 climatological times were calculated, where each one represents an individual month. This procedure preserves all harmonics and only dampens the annual mean.

To better describe the frequencies that could interfere with BMC anomaly formation, statistical analyses based on wavelets were applied to the reanalysis data. The method is the same as that of Torrence and Compo (1998), where the wavelet coherency method was performed on El Niño-Southern Oscillation (ENSO) and monsoon indexes. The wavelet analysis method is used to isolate the different timescales, energies, and phases. In our case, the Morlet wavelet was chosen and the transform was performed in Fourier space using the method described by the same authors. The wavelet cope applied in this work can be found at http://atoc.colorado.edu/research/wavelets/.

### 2.2 Numerical modeling

The Modular Ocean Model version 4 (MOM-4) was developed by the Geophysical Fluid Dynamics Laboratory (GFDL) group, as documented by Griffies et al. (2005). It is a tridimensional, $z$ coordinate, B Arakawa grid, distributed in a tripolar grid with a resolution of 1/3° latitude by 1/3° longitude between 10°N and 10°S, relaxing to 1° latitude by 1° longitude from those latitudes towards the pole. The grid is structured in 50 vertical levels, where the first 22 levels are representative of a depth of 220 m. The maximum depth is 5,500 m. This is a set of Navier-Stokes primitive equations, discretized by finite differences methods and submitted to hydrostatic approximation. These equations are capable of representing most parts of large-scale circulation. MOM-4 uses a series of parameterizations, such as the Smagorinsky scheme (Griffies and Hallberg 2000), to solve the horizontal friction terms, considering the viscosity constant and dependent of the grid. The sea surface elevation is solved by the SPLIT method (Pacanovsky and Griffies 1999), which allows the calculation of oceanic volume through time on the grid surface.

The atmospheric Coordinated Ocean-ice Reference Experiment (CORE) (Large and Yeager 2009) dataset was applied to force MOM-4 in the sensitivity experiments. CORE has a global cover with a horizontal resolution grid of 1° latitude by 1° longitude and a time series spanning from 1958 to 2006 for the synoptic hours. All fluxes were computed from 1984 to 2006. Before 1984, radiation and precipitation were computed only as climatological mean annual cycles (Large and Yeager 2004). Two types of products are available in the GFDL website: the interannual forcing and the normal year forcing. In interannual forcing, the interannual variability is represented in different spatial and temporal timescales, allowing the study of the air-sea interaction process. In contrast, the normal year forcing is the representation of an ideal year, where only the mean annual cycles of daily values are given. The forcing fields applied to this study were air temperature, radiation components, horizontal winds at 10 m, runoff, and humidity. The topography dataset is provided by the Southampton Oceanography Center and is a montage of that developed by Smith and Sandwell (1997), the NOAA 5-min global topography (ETOPO5), and the International Bathymetric Chart of the Arctic Ocean (IBCAO). Temperature (Locarnini et al. 2010) and salinity (Antonov et al. 2010) are provided from the World Ocean Atlas for initial and boundary conditions.

Sets of numerical experiments are designed to simulate the dynamical conditions of SST anomaly appearances in the BMC. The sensitivity experiments were divided into two categories. The first one is called "climatological ocean" and the second simulated the 2 years of interest, 1964 and 1992. These years were chosen because they represent the extreme negative and positive SST anomaly years for the BMC in the SODA dataset. However, the objective of these sensitivity tests is to determine how these anomalies formed and what the main oceanic processes responsible for their formation are. The climatological ocean had forcing conditions from the CORE normal year dataset. It was forced until the solution reached dynamical stability. At the interface, the atmospheric climatological forcings were wind stress, heat fluxes, solar radiation, and water fluxes during the 26 years of spin up. The last simulated year of this experiment was used as the initial condition in the sensitivity tests, and then an anomalous ocean was simulated for the years of 1964 and 1992, forced by the CORE interannual dataset.

## 3 Results and discussion

### 3.1 Time-energy variability analysis

The spectral analysis considering SST anomalies for the BMC region is shown in Fig. 2. SST time series could be divided in two opposite halves related to phase (Fig. 2a). A negative trend is observed in the first half of the time series until the 1970s. From then on, a new positive trend appears, indicating a low-frequency oscillation. This low-frequency behavior was described by Parker et al. (1994) as a strong signal in SST global trends, but low-frequency fluctuations established by positive trends are interspersed with negative trends for the last century. The wavelet spectrum (Fig. 2b), the global wavelet power spectrum (Fig. 2c), and the scale average time series are in agreement (Fig. 2d) when the most energetic period (4 $°C^2$) is approximately 8 years. This trend was observed from the 1980s until the end of the whole time series, with progressively increasing variance from the 1960s to the 1980s. Periods of 2 years, 4 years, and 9 months, in that order, also presented large associated energy. The 2–3-year band is especially relevant from 1975 to 1980 and from 1987 to 1992. This periodicity could be attached to remote effects of El Niño-Southern Oscillation (ENSO). Other studies connected the Southwestern Atlantic with equatorial Pacific conditions. Barreiro and Tippmann (2008) addressed the effect of Atlantic SST anomalies over southeastern South America during January to February, particularly during El Niño years, and showed that the state of the equatorial Atlantic during El Niño years was more important than equatorial Pacific conditions in modulating rainfall. Barros and Silvestri (2002) and Vera et al. (2004) noted the importance of SST variations in the south central Pacific in modulating the influence of El Niño events during spring over the region. However, Witter and Gordon (1999) found an interannual variability of 2–3 years in the BMC by analyzing altimeter data and suggested that this mode corresponded to meridional variations of the latitude of the confluence and to variations in the local distribution of eddy variability linked to changes of the surface

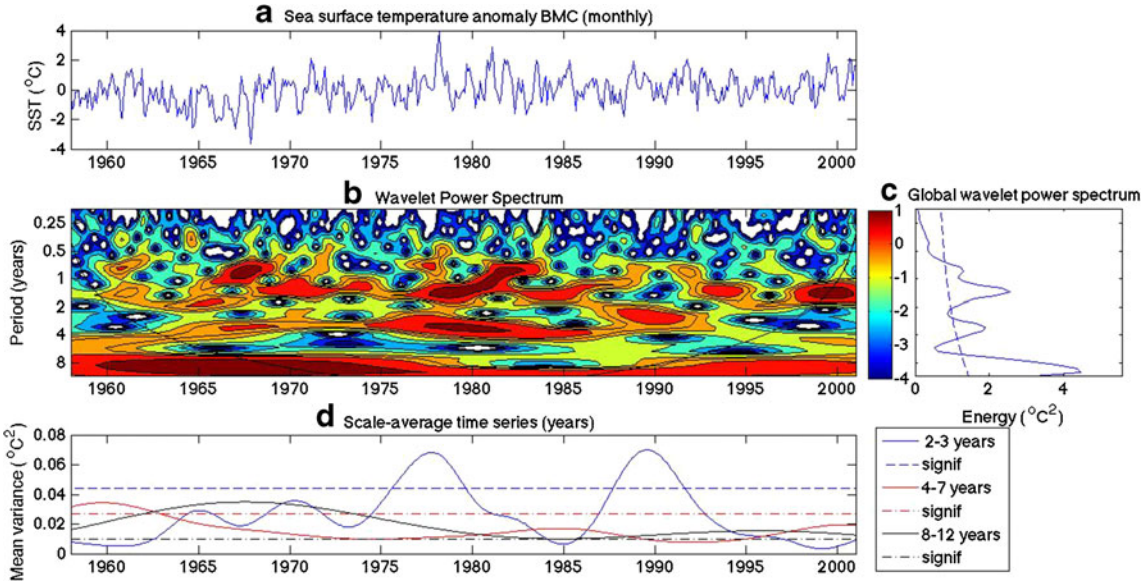


**Fig. 2** Wavelet analysis of sea surface temperature anomalies for BMC. **a** Time series. **b** wavelet power spectrum. **c** Global wavelet power spectrum. In the lower panel (**d**), the *blue line* is the variance of the 2–3-year band, the *red line* is the variance of the 4–7-year band, and the *black line* is the variance of the 8–12-year band. The *dotted lines* represent the significance for each band

velocity of the MC. It is possible that similar mechanisms could drive changes in the SST anomaly.

When zonal wind anomalies are analyzed for the same region (Fig. 3), the 8–12-year band appeared again as the most energetic oscillation in the BMC, with a power of 2.3 $m^2\ s^{-2}$ (Fig. 3c) and a predominant effect after 1985 until the end of the time series (Fig. 3d). Rao et al. (2003) documented a period of 8.33 for baroclinic waves in the meridional wind during the years 1974 to 2000 in their studies on intra-annual variations in the storm track zones in the Southern Hemisphere, and they connected this variability with the Antarctic Oscillation. The second most important signal is at approximately 1 year, where the seasonal signal still appears because first, the annual cycle was partially removed from the original time series, and second, once the wavelet is a symmetrical filter, it cannot completely remove the annual cycle from the spectrum, as demonstrated by Eremy and Thomson (2001). The third period is the 4–7-year band. Although it did not present a large associated energy, it had a great associated variance in 1964–1966 (Fig. 3d). As proposed by Pezzi et al.

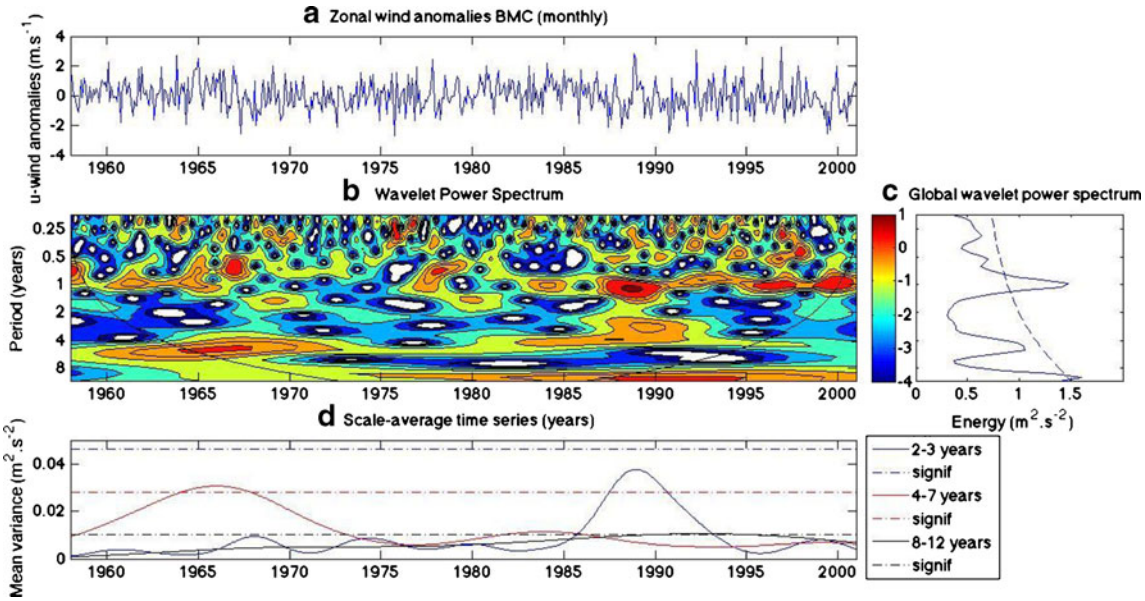


**Fig. 3** Same as Fig. 2 but for zonal wind anomalies at BMC

(2005, 2009), the ocean-to-atmosphere feedback for the BMC region is characterized by a positive correlation between SST and surface wind speed. According to Tokinaga et al. (2005), this positive SST-wind correlation is observed in both spatial and interannual variability.

Ferrari et al. (2012), investigating the Yaghan Basin in the Drake Passage through moorings and altimetry, found a cyclonic eddy at a depth of 2,500 m. This type of mesoscale pattern is possibly one form of connection between surface and deeper layers in this region. The same wavelet technique is used for SST (Fig. 4) and the temperature at a depth of 500 m (Fig. 5) for the Drake Passage region. The aim is to determine the main frequencies that characterize sea temperature variations. The SST anomaly wavelet revealed the importance of 6, 4, 3, 12, and 1.5 years for decreasing energy (Fig. 4c). The 6-year (4–7-year band) period had 3 $°C^2$ and was relevant at the beginning of the time series (1958–1967) and from the mid 1980s to the mid 1990s. The 2–3-year band is important in the mid 1960s, in the 1970s to the mid 1980s, and in the early 1990s. The effects of these two bands appear to have positive synergism in the mid 1960s and in the early 1990s (Fig. 4d). Furthermore, the same periods were observed for temperatures at a depth of 500 m (Fig. 5). Among the periods, the 2–3-year band presented a larger variance than the 4–7-year band between 1985 and 1995, which could indicate that the energy of the 4–7-year band was transferred from the surface to deeper levels and that of the 2–3-year band was transferred in the opposite direction for the years 1985–1995.

SST anomalies in the BMC (Fig. 2) and Drake Passage (Fig. 4) present opposite phases when compared. The opposite situation was documented by Vivier et al. (2001), where the SST variability in the MC region occur in phase with the propagation of the Antarctic circumpolar current (ACC) as a shelf break wave. Although the wavelet analysis shows great activity between the 1980s and 2000 in almost every period, the most energetic waves have a period of 6–8 years. Those waves are present in the Drake Passage water column from the surface to a depth of 500 m, which may be related to ACC propagation characteristics and fluctuations. This finding contributes to the idea that anomalous thermal processes that occur at the BMC surface are linked to processes in the Drake Passage. This result agrees with that of Vivier et al. (2001), who found that variability in MC seasonal and intraseasonal (approximately 70 days) transport connected remotely to wind stress curl anomalies in the Drake Passage. These results were further assessed using a 5-year series of transport in the MC derived from altimeter data. However, the low-frequency variability shown in our paper could not be explained by the mechanisms described by Vivier et al. (2001).

In this context, Barrucand et al. (2008) showed an 8-year periodicity wave, which presents a positive phase with the Antarctic Oscillation (AAO), in the Atlantic SST until the 1990s. This finding agreed with the positive SST anomalies along the Southwestern Atlantic shore. Part of this change in the sea temperature of mid latitudes is bounded by the changes in zonal wind shown in Fig. 3, where the 8-year period is the most energetic.

### 3.2 SST and dynamical analysis

In this section, the results of MOM-4 climatology and sensitivity test experiments are discussed. The oceanic climatological simulation was able to describe the main patterns and features of the BMC when compared to the literature (Romero

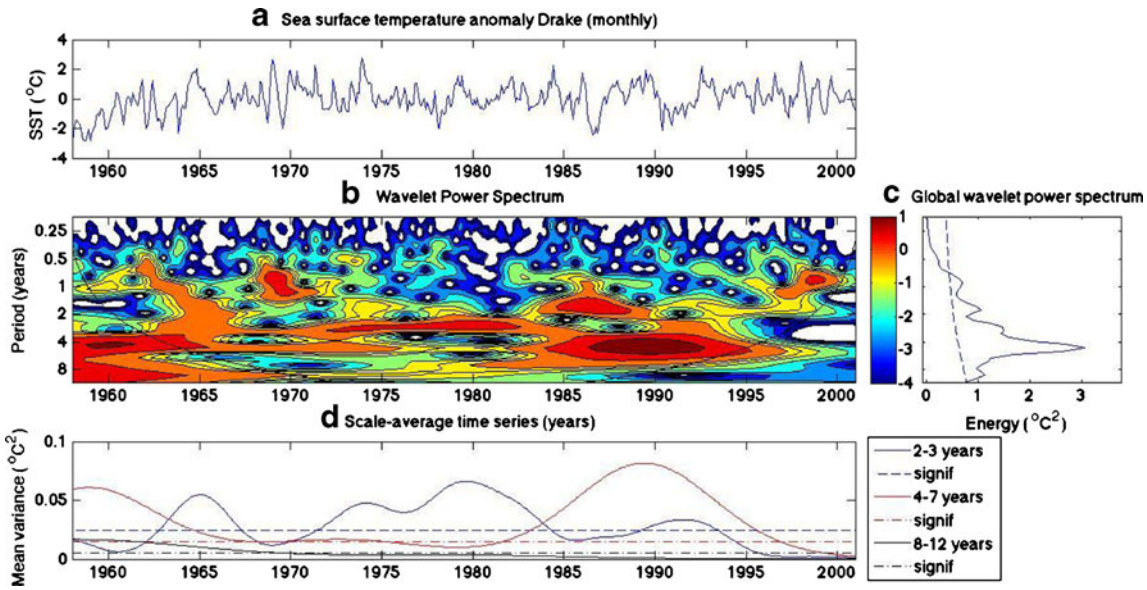


**Fig. 4** Similar to Fig. 2 but for the time series for SST anomalies at Drake Passage

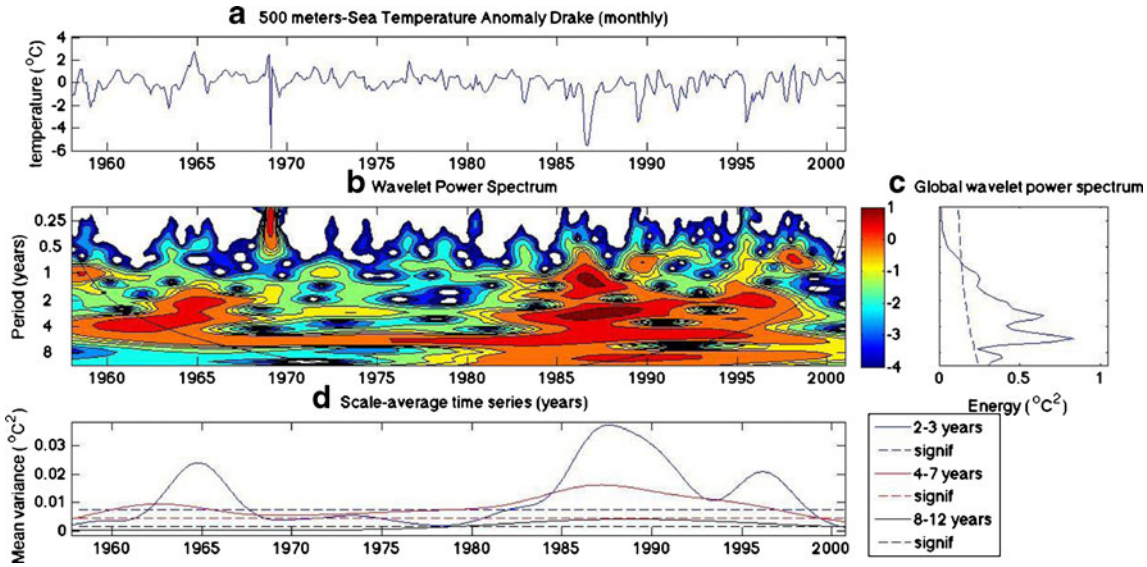


**Fig. 5** Same as Fig. 2 but for the time series of sea temperature anomalies at a depth of 500 m in Drake Passage

et al. 2006; Möller et al. 2008; Palma et al. 2008; Pezzi et al. 2009). The model reproduced a similar summer climatological profile (Fig. 6) to that described by Möller et al. (2008) in their Fig. 10b. Figure 6 presents the main water masses distributed from the surface to a depth of 300 m for the austral summer climatological season, but it fails to separate the South Atlantic central water (SACW) from subantarctic shelf water (SASW). The model also failed to represent the salinity range of the Plata plume water (PPW), as Möller et al. (2008) found PPW salinity between 26 and 33.5. The MOM-4 climatology water column profile presented the warmer and saltier BC waters (20 °C, 36) as being transported southward between 52°W and 46°W at depths of up to 250 m (not shown). Below the BC, an oceanic front was observed, characterized by a strong temperature gradient similar to those observed by Pezzi et al. (2009) (not shown). Near 38°S, the BC advection was approximately 30 Sv during the austral summer in the upper 200 m. This value agrees with those found by Gordon and Greengrove (1986) and Peterson and Stramma (1991). The MC transport through the north was calculated for the upper 500 m and shows a systematic transport decrease from higher to lower latitudes, starting with 80 Sv at 45°S, followed by 35 Sv at 41°S and 10 Sv at 38°S (not shown).

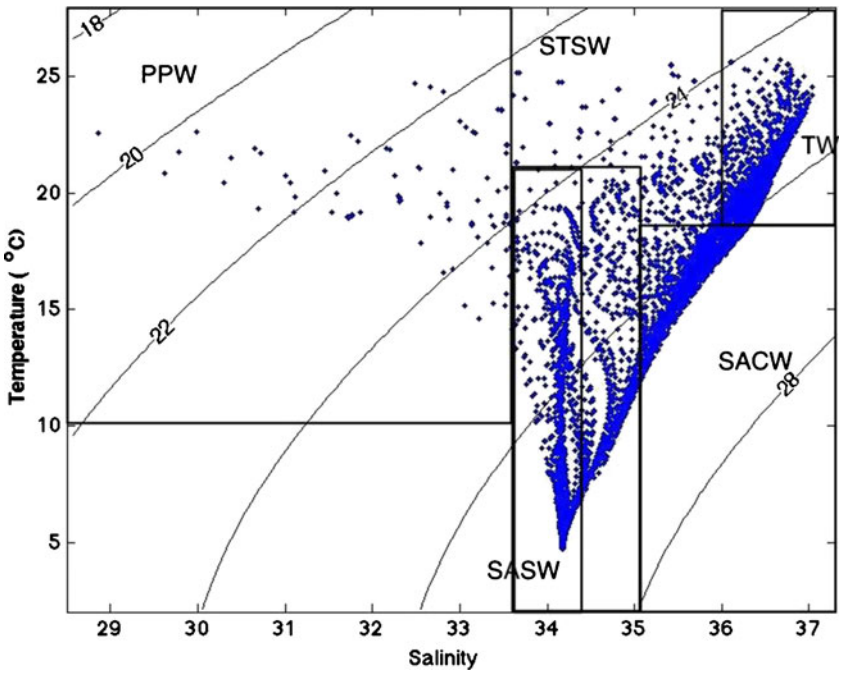


**Fig. 6** MOM-4 climatological TS diagram for austral summer: water masses are Plata plume water (*PPW*), subantarctic shelf water (*SASW*), subtropical shelf water (*STSW*), South Atlantic central water (*SACW*) and tropical water (*TW*)

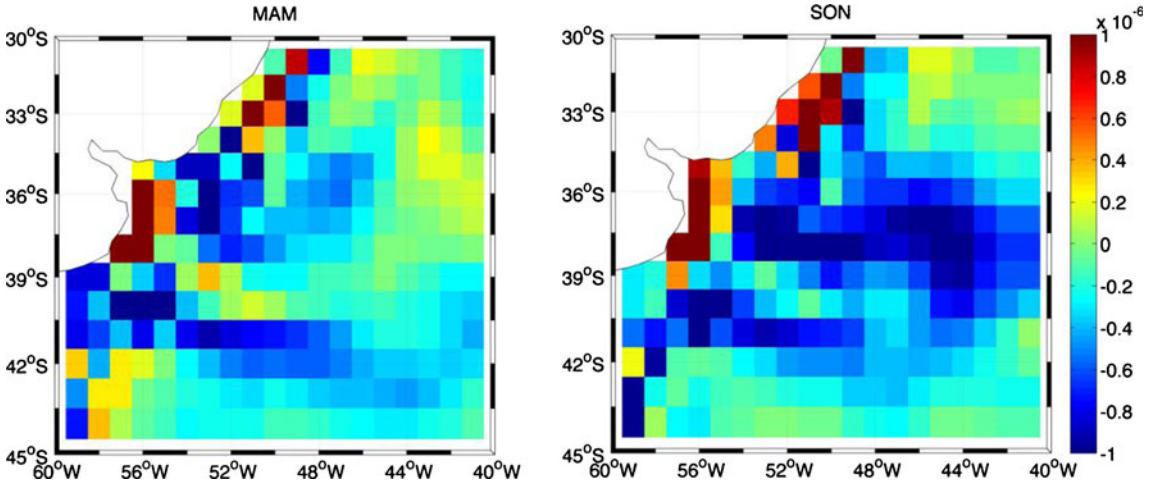


**Fig. 7** MOM-4 climatological vertical velocity (in meters per second) for austral fall and sprin

During austral fall (MAM), negative vertical velocities are observed over the continental shelf and next to the MC retroflexion (Fig. 6). This circumstance produces cold subantarctic water and Río de la Plata fresh water intrusions on the shore. Similar results were described by Möller et al. (2008). In the climatological austral spring (SON) (Fig. 7), the model simulated an upwelling region near the continental slope and offshore. These features are in accordance with model results from Palma et al. (2008), who validated their results with satellite observations of phytoplankton blooms observed by

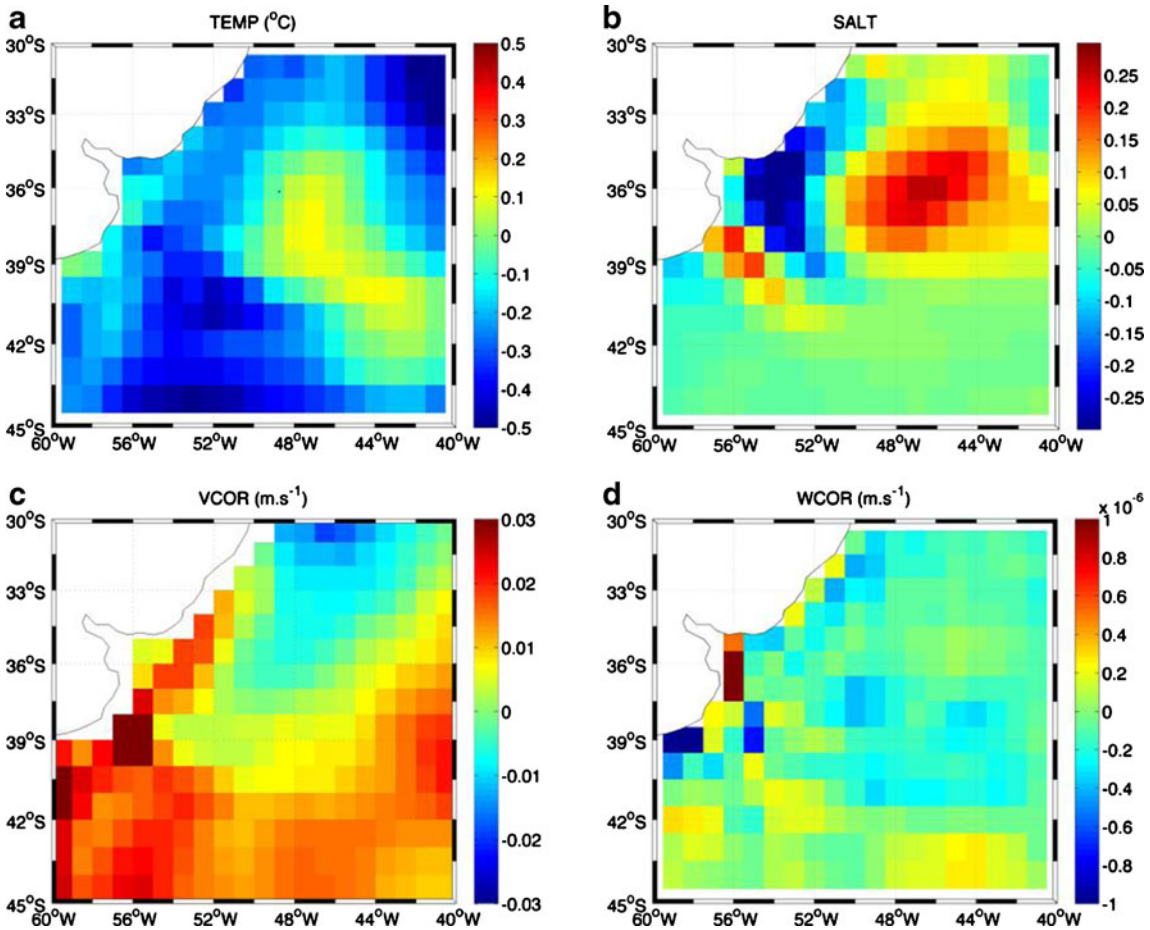


**Fig. 8** MOM-4 surface monthly mean analysis for February, March and April 1964. **a** SST anomalies (in degrees Celsius). **b** Salinity anomalies. **c** Meridional velocity (in meters per second). **d** Vertical velocity (in meters per second)

other researchers in the region. Their analysis also indicated a northward middle-shelf current linked to the MC that interacted with the BC and with the Brazilian shelf topography, inducing shelf break upwelling.

The negative and the positive SST anomaly events in the BMC are represented by the years 1964 and 1992, respectively. The main waves that occurred in those years can be observed in Fig. 2. Both years are modulated by the 2–3-year band and 8–12-year band (Fig. 2d). However, the difference between them is that for 1964, the 8–12-year band is more important than the 2–3-year band, with a variance of 0.035 $°C^2$. For the year 1992, the main band is 2–3-years, with a variance of 0.05 $°C^2$. These results suggest that in both years, the SST anomalies in the BMC were driven by the same forces with different participation. Both years also appear to be influenced by ENSOs, according to the past event ENSO indexes on the International Research Institute for Climate and Society (http://iri.columbia.edu/climate/ENSO/background/pastevent.html) Web site. The year of 1964 was characterized as La Niña and 1992 as El Niño. This evidence indicates that ENSO may have affected the BMC SST anomalies.

The sensitivity test for the year 1964 was characterized by negative sea temperature anomalies in most of the BMC (Fig. 8a). However, the results of this study report the months of February, March, and April. A positive temperature anomaly core (Fig. 8a) associated with a positive salinity anomaly (Fig. 8b) was observed in the center of the region. This feature can be associated with the vertical structure present in Fig. 9a, b. The most negative salinity anomalies are located in the Río de la Plata discharge zone (Fig. 8b), indicating its contribution to water mass modification. Through application of MODIS images, Barré et al. (2006) described the occurrence of two thermal fronts in the BMC: one corresponding to the BC southernmost limit and the other to the MC northernmost limit. These two fronts remained in continental shelf waters with intermediate temperatures (18 °C) and an extremely high chlorophyll-a concentration (up to 4 mg $m^{-3}$). However, the Río de la Plata contribution could be underestimated because of the model's difficulty in reproducing its contribution to salinity climatology, as explained above. When upper meridional circulation occurs, as shown in Fig. 8c, a northward flow can be seen along the shelf break further north of 33°S. Under this regime, the BC influence is limited to lower latitudes. Palma et al. 2008 reported that for austral summer, the northern part of the BMC was influenced by onshore intrusions of BC waters and by the retraction of the La Plata plume. The end summer/fall of 1964 was an anomalous year under the

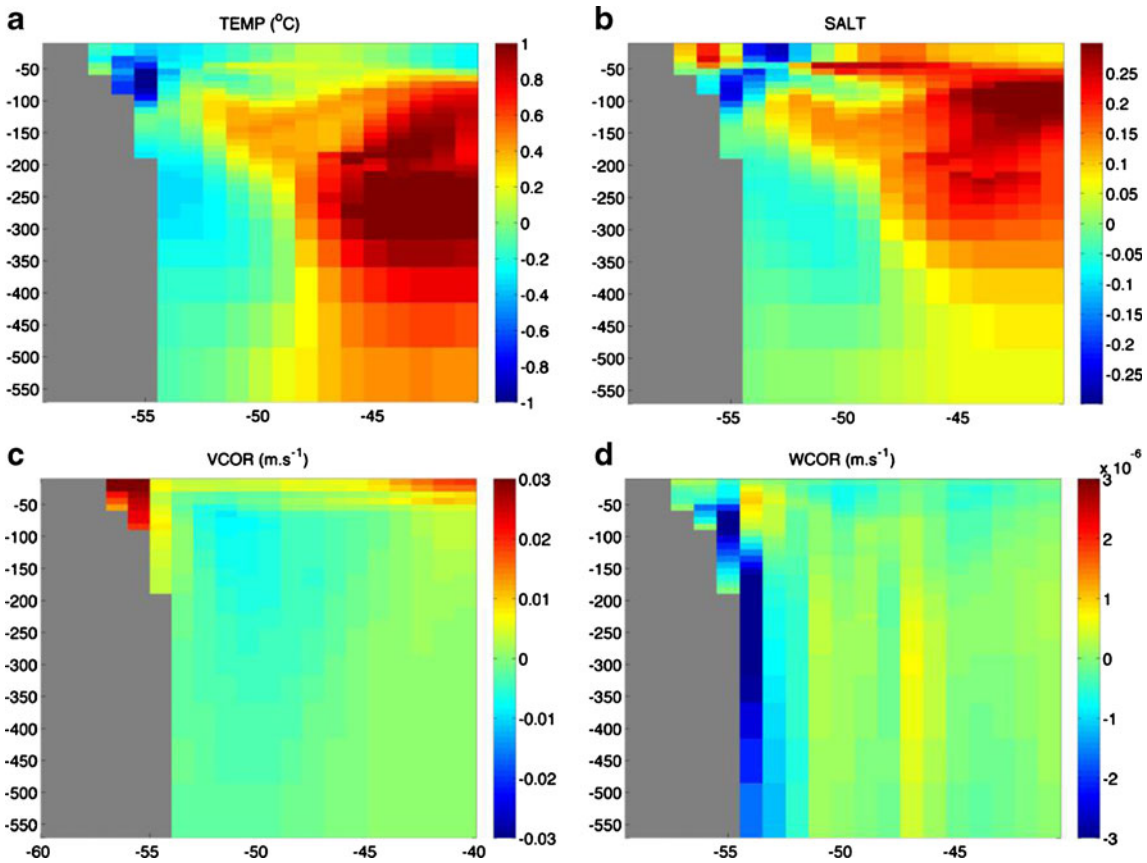


**Fig. 9** Same as Fig. 8, but for the vertical profile at 38°S

Palma et al. (2008) characterization. Furthermore, attached to this anomalous cold northward flow, negative vertical velocities developed along the shore and offshore (36°S and 39°S), apparently contributing to negative SST and salinity anomalies (Fig. 8d).

The water column profiles for 38°S indicate that negative salinity and temperature anomalies are isolated in the upper 100 m and along the slope (Fig. 9a, b). At this depth, a well-defined thermal front is observed to separate positive anomalies from the surface (Fig. 9a). At this same depth, positive salt anomalies are observed, suggesting the existence of salt fingers (Fig. 9b). Bianchi et al. (2002) described the existence of high-salt-finger activity extending along the first 400 dbar in the BMC, using CTD data, and also suggested that double diffusive processes and salt fingers affect approximately 80 % of the upper 400 m of the water column because of saline fluxes. Positive meridional velocity anomalies occur along the shelf break (Fig. 8c), illustrating a northward flow between the surface and a depth of 100 m (Fig. 9d). Palma et al. (2008), applying numerical modeling, found an upstream influence of the MC beyond its retroflexion, in the form of a northward middle-shelf current. When this current interacted with the BC and with local topography, it induced shelf break upwelling (Palma et al. 2008). Some spots of negative vertical velocity appear on the inner shelf (Fig. 8d), extending down to a depth of 600 m (Fig. 9d). This negative vertical velocity anomaly appears to be the local force that drives negative temperature and salt anomalies to the surface. Lentini et al. (2001) studied SST anomalies over a larger region that included the BMC from 1982 to 1994 and found that more than 65 % of the total non-seasonal variance suggested that cold SST anomalies were related to ENSO events. They also noted that the anomalous cold water extensions on the shelf in the north occur generally in every warm ENSO +1 year in the climatology data. Their hypothesis could be applied as a possible remote mechanism that may explain the 1964 cold event in this study, whereas 1963 was an El Niño year. Nevertheless, 1964 also featured other waves beyond the ENSO signal.

The year 1992 presented positive SST anomalies across all periods (not shown). SST anomalies for three monthly means (February, March, and April) can be observed in Fig. 10a, ranging from 0.2 °C to over 1 °C in most areas. A negative

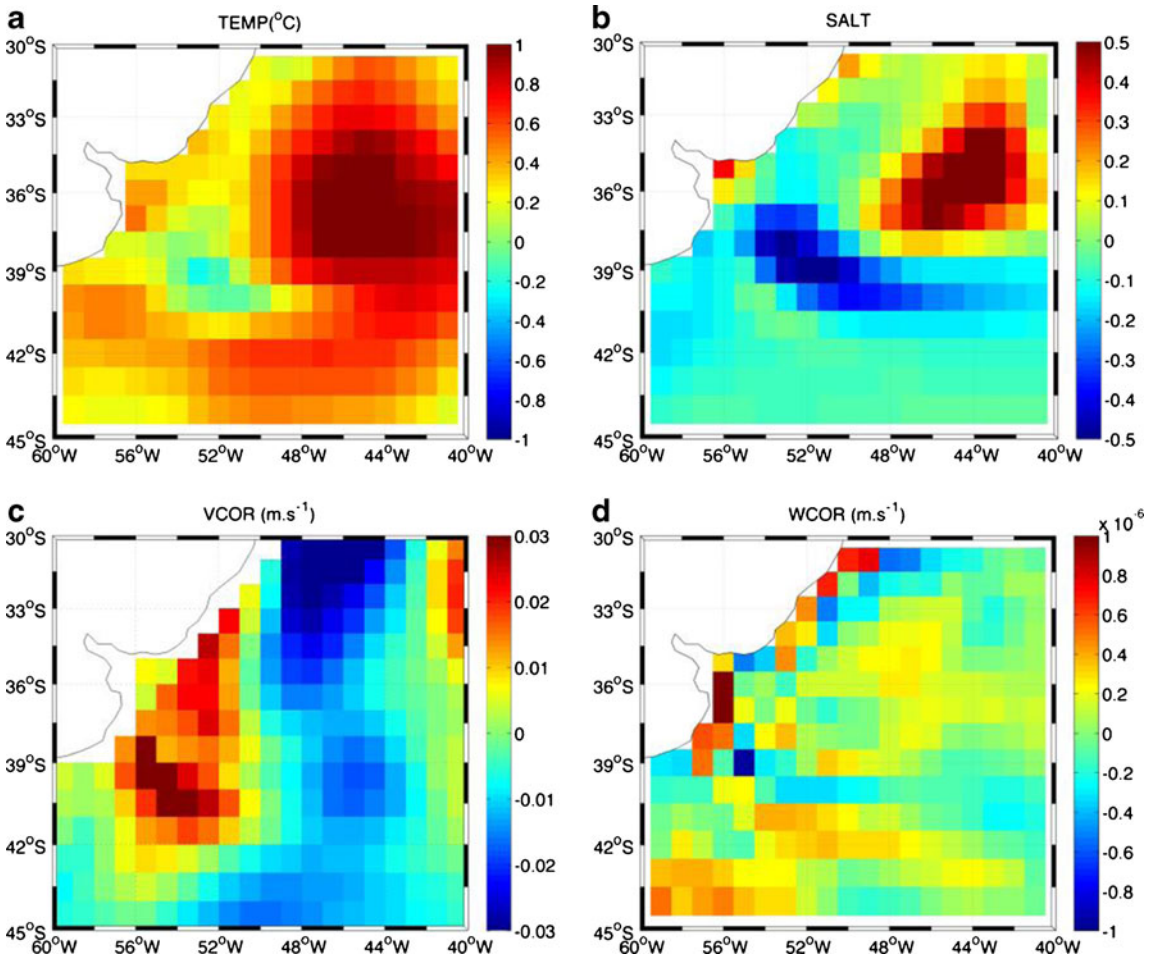


**Fig. 10** MOM-4 surface monthly mean analysis for February, March and April 1992. **a** SST anomalies (in degrees Celsius). **b** Salinity anomalies. **c** Meridional velocity (in meters per second). **d** Vertical velocity (in meters per second)

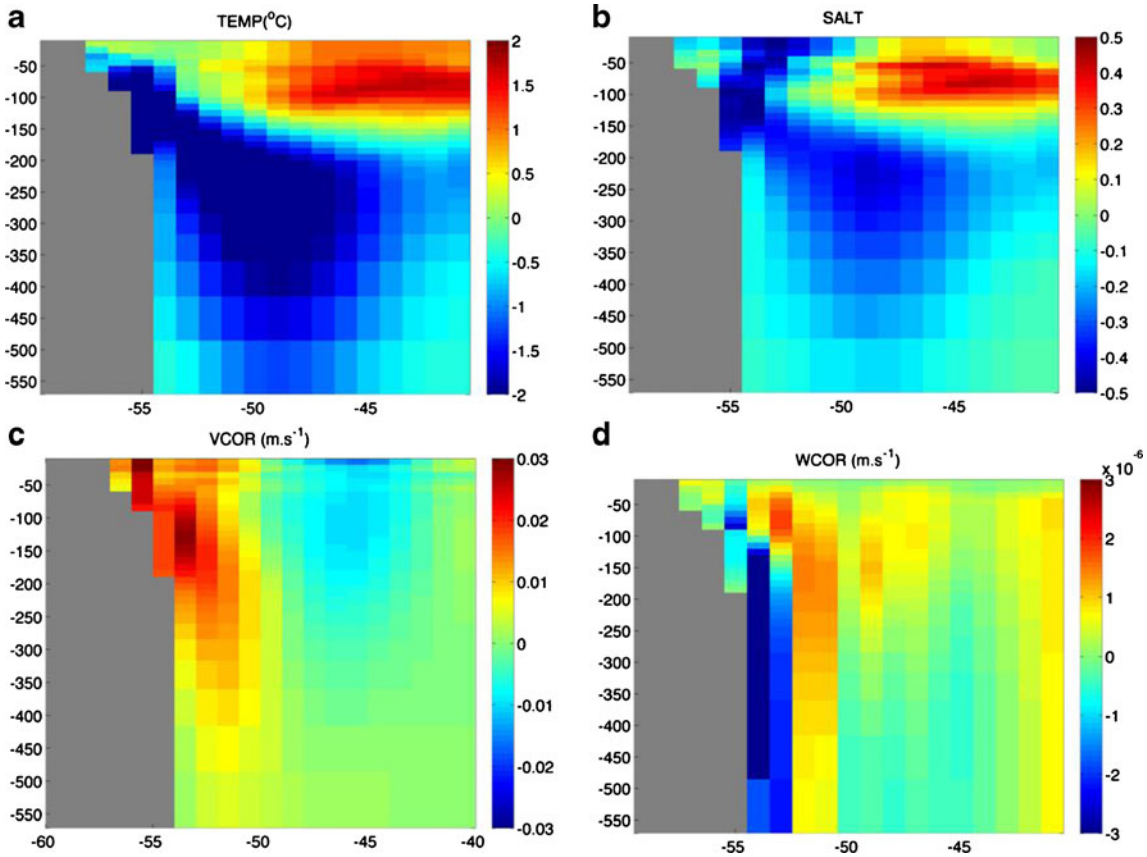


**Fig. 11** Same as Fig. 10, but for the vertical profile at 38°S

core (−0.2 °C) is observed near 40°S, 54°W and could be associated with negative salinity anomalies (Fig. 10b). The same association could be made between the positive SST core and the position of higher positive values in salinity. The positive SST signal appears to be linked to negative meridional transport anomalies (from north to south), adding to the BC contribution (Fig. 10c). However, the negative core corresponds to a southern intrusion (Fig. 11c) or to upwelling processes, as seen in Figs. 10d and 11d.

When the water column is observed, positive anomalies of temperature and salinity are confined to the upper 120 m (Fig. 11a, b), even though the negative temperature anomalies extend from the surface to a depth of more than 600 m, indicating the modification of intermediate waters transported by the MC. These waters are trapped under a thermal front, except on the 55°W, where the upwelling exposes them to the surface (Fig. 11d). Downwelling occurs along the region where the positive anomalies are present (Fig. 11d). At 38°S, the meridional transport points to MC intensification next to the continental slope (Fig. 11c). This pattern helped to generate negative temperature anomalies in 1964. However, in 1992, this effect was lessened, perhaps by the Río de la Plata discharge. The negative SST anomalies occur at levels deeper than 50 m, although the negative salinity anomalies spread out in the inner shelf. Lentini et al. (2001) described the year 1992 as consisting of southward-advected SST cold anomalies with no observed coherent surface patterns. However, they observed that these anomalies reached the southernmost latitude of 31°S in February and March of 1992 with speeds of 13 cm $s^{-1}$ and persisted over 60 days.

Note that in both cases, temperature and salinity anomalies are trapped in the upper meters of the water column, followed by vertical inversion of the signal. In the 1964 sensitivity test, the negative layer overlaps the positive, characterizing thermal inversion and vertical instability. The negative SST anomalies are less intense than the positive anomalies and also more dynamical. Furthermore, positive SST anomalies in 1992 are also detached from the rest of the water column, and this effect tends to be persistent and stable.

## 4 Conclusions

SST anomalies in the BMC region were investigated by two different approaches. The first approach aimed to find the main periodicities of SST anomaly events at the BMC and their associated energy through application of wavelet analysis. The second approach was to find possible dynamical answers to the appearance of colder and warmer anomalies in the CBM using a numerical model.

As shown by the wavelet analysis, the BMC and Drake Passage SST anomalies presented opposite phases but the same energetic band of 8–12 years. This band was also present in the zonal wind anomalies for the BMC, suggesting air-sea-coupled processes. These periods are consistent with the Southern Annular Mode (SAM) or Antarctic Oscillation, which is the leading mode of low-frequency variability in the Southern Hemisphere (Thompson and Wallace 2000). This mode explains approximately 27 % of the total variance and is characterized by a strong zonal symmetry with a phase reversal between high and middle latitudes, and with an imprint of zonal wavenumber 2 and wavenumber 3 (Kidson 1999). The SAM appears year-round, although it is more active during austral spring when it is amplified upward into the stratosphere (Thompson and Wallace 2000). Other important frequencies were exposed by the wavelet analysis. For the BMC, the periods of 1.5, 2, and 3.5–4 years also appeared in the SST with significant associated energy. However, for zonal wind, the period of approximately 1 year seems to be more important, followed by 8 and 4 years. Those periods could indicate that other remote forcing of the SST anomalies at the BMC could be linked to ENSO patterns, as demonstrated by other researchers. Wavelets for SST and temperature at 500 m from the Drake Passage show the same periods: approximately 1, 2, 3, and 5.5 years. The BMC SST anomaly wavelet for the year 1964 shows significant mean variances for the bands of 2–3 years (0.02 $°C^2$) and 8–12 years (0.037 $°C^2$). Although the same bands appear significant for the year 1992, the variances are 0.065 $°C^2$ for the 2–3-year band and 0.02 $°C^2$ for the 8–12-year band. These results suggest that the main remote forces for the BMC in 1964 and 1992 are both SAM and ENSO, but the order of importance shifted from SAM to ENSO in 1964 to ENSO to SAM in 1992.

The sensitivity tests for the years1964 and 1992 (cold and warm ENSO phases) are presented in section 3.2. The model result shows that the SST anomalies that arise in the BMC result from combined local forcing: zonal advection, upwelling, and runoff rates. For the negative episode during 1964 austral autumn, negative SST anomalies are associated with three different parameters: northward cold advection, Río de la Plata discharge, and upwelling. This negative northward cold advection was revealed by Palma et al. (2008) and is characterized by the formation of a distinct oceanic flow, known as the Patagonian Current, which is generated by the combined effects of low-salinity discharges from Magellan Straits, tidal mixing, and wind stress forcing over the Argentinean Basin. However, positive SST anomalies registered in 1992 are attached to a BC southward excursion and a decrease in upwelling processes. In addition to these processes, the Río de la Plata discharge appears to contribute to local buoyancy through negative alterations in salinity distribution. However, the positive SST anomalies seem to also be forced by atmospheric parameters.

This work is a first attempt to answer this specific question about warm and cold anomalous water events. The physical mechanisms found in this study to explain the appearance of such anomalies are the northward cold flow and upwelling for 1964 and a southward excursion of the Brazil Current (BC) front in 1992. Results found for both years suggest that the alterations in the Río de la Plata discharge rates might be playing a role on this mechanism. This topic, however, needs additional studies using other tools such as regional numerical models with river discharge in it or using in situ data. The role of air-sea interactions through heat fluxes is also another issue arisen by our numerical results, since the anomalies are trapped in the first tens of meters of depth. These results also should be investigated deeply, such as analyzing their correlations with remote forcing such as ENSO and SAM.

**Acknowledgments** We would like to thank the National Institute for Space Research (INPE), the National Counsil of Technological and Scientific Development (CNPq), and São Paulo Research Foundation (FAPESP) for their support. The first author was funded by FAPESP 2007/06782-0 and Atlantic Carbon Experiment (ACEx-CNPq) 558108/2009–1. Luciano Ponzi Pezzi acknowledges support from CNPq, as a contribution for the PQ (CNPq) project number 304633/2012-7. Two anonymous reviewers provided comments, which reflected substantial improvements to this paper.

## References

Acevedo OC, Pezzi LP, Souza RB, Anabor V, Degrazia G (2010) Atmospheric boundary layer adjustment to the synoptic cycle at the Brazil-Malvinas Confluence South Atlantic Ocean. J Geophys Res 115: D22107. doi:10.1029/2009JD013785

Alexander MA, Penland C (1996) Variability in a mixed layer model of the upper ocean driven by stochastic atmospheric surface fluxes. J Climate 9:2424–2442

Antonov JI, Seidov D, Boyer TP, Locarnini RA, Mishonov AV, Garcia HE (2010) World ocean atlas 2009 volume 2: salinity. In: Levitus S (ed) NOAA atlas NESDIS 69. U.S. Government Printing Office, Washington, D.C

Barré N, Provost C, Saraceno M (2006) Spatial and temporal scales of the Brazil–Malvinas Current confluence documented by simultaneous MODIS Aqua 1.1-km resolution SST and color images. Adv Space Res 37:770–786

Barreiro M, Tippmann A (2008) Atlantic modulation of El Niño influence on summertime rainfall over southeastern South America. Geophys Res Lett 35. doi:10.1029/2008GL035019. issn: 0094-8276

Barros VR, Silvestri GE (2002) The relation between sea surface temperature at the subtropical south-central Pacific and precipitation in southeastern South America. J Climate 15:251–267

Barrucand M, Rusticucci M, Vargas W (2008) Temperature extremes in the south of South America in relation to Atlantic Ocean surface temperature and Southern Hemisphere circulation. J Geophys Res 113: D20111. doi:10.1029/2007JD009026

Bianchi AA, Giulivi CF, Piola AR (1993) Mixing in the Brazil/Malvinas Confluence. Deep-Sea Res 40:1345–1358

Bianchi AA, Piola AR, Collino GJ (2002) Evidence of double diffusion in the Brazil–Malvinas Confluence. Deep-Sea Res I 49:41–52

Bonatti JP, Rao VB (1999) Meso escale perturbations and thermohaline fronts in the South Atlantic Ocean. Dyn Atmos Oceans 30:11–24. doi:10.1016/S0377-0265(99)00016-0

Carton AG, Giese BS (2008) A reanalysis of ocean climate using simple ocean data assimilation (SODA). Mon Weather Rev 136:2999–3017

Carton AG, Chepurin G, Cao X, Giese BS (2000) A simple ocean data assimilation analysis of the global upper ocean 1950–95. Part I: methodology. J Phys Oceanogr 30:294–309

Chelton DB, Schlax MG, Witter DL, Richman JG (1990) GEOSAT altimeter observations of the surface circulation of the Southern Ocean. J Geophys Res 95:17,877–17,903. doi:10.1029/JC095iC10p17877

Conkright ME, Locarnini RA, Garcia HE, O'Brien TD, Stephens CM, Antonov JI (2002) World Ocean Atlas 2001: objective analyses, data statistics, and figures. Natl Oceanogr Data Center, Silver Spring (17)

Corre L, Terray L, Balmaseda M, Ribes A, Weaver A (2010) Can oceanic reanalysis be used to assess recent anthropogenic changes and low-frequency internal variability of upper ocean temperature? Clim Dyn 38:877–896

Cunningham AP, Barker PF (1996) Evidence for westward-flowing Weddell Sea deep water in the Falkland Trough, western South Atlantic. Deep-Sea Res 43:643–654

de Camargo R, Todesco E, Pezzi LP, de Souza RB (2013) Modulation mechanisms of marine atmospheric boundary layer at the Brazil-Malvinas Confluence region. J Geophys Res Atmos 118. doi:10.1002/jgrd.50492

Diaz AF, Studzinski CD, Mechoso CR (1998) Relationships between precipitation anomalies in Uruguay and Southern Brazil and sea surface temperature in the Pacific and Atlantic Oceans. J Climate 11:251–271

Eremy WJ, Thomson RE (2001) Data analysis methods in physical oceanography. 2nd ed. Elsevier, 638 p

Ferrari R, Provost C, Renault A, Sennéchael N, Barré N, Park Y-H, Lee JH (2012) Circulation in Drake Passage revisited using new current time series and satellite altimetry: 1. The Yaghan Basin. J Geophys Res 117, C12024, doi:10.1029/2012JC008264

Fetter AFH and Matano R (2008) On the origins of the variability of the Malvinas Current in a global, eddy-permitting numerical simulation. J Geophys Res 113, C11018. doi:10.1029/2008JC004875

Gan MA, Rao VB (1991) Surface cyclogenesis over South America. Mon Weather Rev Notes Correspondence 119:1293–1303

Garcia CAE, Sarma YVB, Mata MM, Garcia VMT (2004) Chlorophyll variability and eddies in the Brazil-Malvinas Confluence region. Deep-Sea Res 51:159–172

Garzoli SL, Giulivi C (1994) What forces the variabillity of the southwestern Atlantic boundary currents? Deep-Sea Res I 41:1527–15550

Garzoli SL, Gordon AL (1996) Origins and variability of the Benguela Current. J Geophys Res 101:897–906

Garzoli SL, Matano R (2011) The South Atlantic and the Atlantic meridional overturning circulation. Deep-Sea Res II 58:1837–1847

Goni G, Wainer I (2001) Investigation of the Brazil Current front dynamics from altimeter data. J Geophys Res 106:31,117–31,128. doi:10.1029/2000JC000396

Gordon AL, Greengrove CL (1986) Geostrophic circulation of the Brazil-Falkland Confluence. Deep Sea Res Part A 573–585

Griffies SM, Hallberg RW (2000) Biharmonic friction with a smagorinsky-like viscosity for use in large-scale eddy-permitting ocean models. Mon Weather Rev 128:2935–2946

Griffies SM, Gnanadesikan A, Dixon KW, Dunne JP, Gerdes R, Harrison MJ, Rosati A, Russell JL, Samuels BL, Spelman MJ, Winton M, Zhang R (2005) Formulation of an ocean model for global climate simulations. Ocean Sci 1:45–79

Hoskins BJ, Hodges KIA (2005) A new perspective on Southern Hemisphere storm tracks. J Climate 18:4108–4130

Katsumata K, Masuda S (2013) Variability in Southern Hemisphere ocean circulation from the 1980s to the 2000s. J Phys Oceanogr 43(9):1981–2007

Kidson JW (1999) Principal modes of Southern Hemisphere low frequency variability obtained from NCEP-NCAR reanalysis. J Climate 12: 2808–2830

Klein B, Molinari RL, Muller TJ, Siedler G (1995) A transatlantic section at 14.5°N: meridional volume and heat fluxes. J Mar Res 53:929–957

Large WG, Yeager S (2004) Diurnal to decadal global forcing for ocean and sea-ice models: the data sets and flux climatologies. NCAR Technical Note: NCAR/T-460+STR. CGD Division of the National Center for Atmospheric Research, USA

Large WG, Yeager S (2009) The global climatology of an interannually varying air-sea flux data set. Clim Dyn 33:341–364. doi:10.1007/s00382-008-0441-3

Legeckis R, Gordon AL (1982) Satellite observations of the Brazil and Falkland Currents—1975 to 1976 and 1978. Deep-Sea Res 29:375–401

Lentini CAD, Podestá GG, Campos EJD, Olson DB (2001) Sea surface temperature anomalies on the western South Atlantic from 1982 to 1994. Cont Shelf Res 21:89–112

Locarnini RA, Mishonov AV, Antonov JI, Boyer TP, Garcia HE (2010) World ocean atlas 2009, volume 1: temperature. In: Levitus S (ed) NOAA atlas NESDIS 68. U.S. Government Printing Office, Washington, D.C, 184 pp

Lübbecke JF, McPhaden MJ (2013) A comparative stability analysis of Atlantic and Pacific Niño modes. J Climate 26(16):5965–5980

Maamaatuaiahutapu K, Garçon VC, Provost C, Boulahdid M, Osiroff AP (1992) Brazil-Malvinas Confluence: water mass composition. J Geophys Res 97:9493–9506

Matano RP, Schlax MG, Chelton MG (1993) Seasonal variability in the southwestern Atlantic. J Geophys Res 98:18,027–18,035

Möller OO, Piola AR, Freitas AC, Campos AJD (2008) The effects of river discharge and seasonal winds on the shelf o southeastern South America. Cont Shelf Res 28:1607–1624. doi:10.1016/j.csr.2008.03.012

Namias J, Born RM (1974) Further studies of temporal coherence in North Pacific sea surface temperatures. J Geophys Res 79:797–798

Olson D, Podesta G, Evans R, Brown O (1988) Temporal variations in the separation of the Brazil and Malvinas Currents. Deep-Sea Res 35:1971

Pacanovsky RC, Griffies SM (1999) "The MOM 3 manual," Geophys Fluid Dynam Labor, NOAA Princenton

Palma ED, Matano RP, Piola AR (2008) A numerical study of the Southwestern Atlantic Shelf circulation: stratified ocean response to local and offshore forcing. J Geophys Res 113:1–22. doi:10.1029/2007JC004720, C11010

Parker DE, Jones PD, Folland CK, Bevan A (1994) Interdecadal changes of surface temperature since the late nineteenth century. J Geophys Res 99:14373–14399

Peterson RG, Stramma L (1991) Upper-level circulation in the South Atlantic Ocean. Prog Oceanogr 26(1):1–73

Pezzi LP, Cavalcanti I (2001) The relative importance of ENSO and tropical Atlantic sea surface temperature anomalies for seasonal precipitation over South America: a numerical study. Clim Dyn 17:205–212

Pezzi LP, Souza RB, Dourado MS, Garcia CAE, Mata MM, Silva-Dias MAF (2005) Ocean-atmosphere in situ observations at the Brazil-Malvinas Confluence region. Geophys Res Lett 32: L22603, doi:10.1029/2005GL023866

Pezzi LP, Souza RB, Acevedo O, Wainer I, Mata MM, Garcia CAE, Camargo R (2009) Multi-year measurements of the oceanic and atmospheric boundary layers at the Brazil-Malvinas Confluence region. J Geophys Res 114:D19103. doi:10.1029/2008JD011379

Piola AR, Matano RP (2001) In: Thorpe SA (ed) Brazil and Falklands (Malvinas) Currents. Encyclopedia of ocean sciences. Elsevier, New York, pp 340–349

Piola AR, Campos EJD, Möller OO, Charro M, Martinez C (2000) The Subtropical shelf front off eastern South America. J Geophys Res 105:6565–6578

Provost C, Garçon V, Falcon LM (1996) Hydrographic conditions in the surface layers over the slope-open ocean transition area near the Brazil-Malvinas Confluence during austral summer 1990. Cont Shelf Res 162:215–219

Rao VB, Do Carmo A, Franchito S (2003) Interannual variations of the storm tracks in the Southern Hemisphere and their connections with the Antarctic Oscillation. Int J Climatol 23:1537–1545. doi:10.1002/joc.948

Romero SL, Piola AR, Charo M, Garcia CE (2006) Chlorophyll-a variability off Patagonia based on SeaWiFS data. J Geophys Res 111: C05021 doi:10.1029/2005JC003244

Saraceno M, Provost C, Piola AR, Bava J, Gagliardini A (2004) Brazil Malvinas Frontal System as seen from 9 years of advanced very high resolution radiometer data. J Geophys Res 109: C05027, doi:10.1029/2003JC002127

Smith WHF, Sandwell DT (1997) Global seafloor topography from satellite altimetry and ship depth soundings. Science 277:1957–1962

Souza RB, Mata MM, Garcia CAE, Kampel M, Oliveira EN, Lorenzzetti JA (2006) Multisensor satellite and in situ measurements of a warm core eddy south of the Brazil-Malvinas Confluence region. Remote Sens Environ 100:52–66. doi:10.1016/j.rse.2005.09.018

Spadone A, Provost C (2009) Variations in the Malvinas Current volume transport since 1992. J Geophys Res 114, C02002. doi:10.1029/2008JC004882

Thompson DWJ, Wallace JM (2000) Annular mode in the extratropical circulation. Part I: month-to-month variability. J Climate 13:1000–1016

Tokinaga H, Tanimoto Y, Xie S-P (2005) SST-induced wind variations over Brazil-Malvinas Confluence: satellite and in-situ observations. J Climate 18:3470–3482

Torrence C, Compo GP (1998) A practical guide to wavelet analysis. Bull Am Meteorol Soc 79(1):61–78

Trenberth KE (1997) The definition of El Niño. Bull Am Meteorol Soc 78:2771–2777

Trenberth KE, Stepaniak DP (2001) Indices of El Niño evolution. J Climate 14:1697–1701

Venegas SA, Mysak LA, Straub DN (1996) Evidence for interannual and interdecadal climate variability in the South Atlantic. Geophys Res Lett 23:2673–2676

Vera C, Silvestri G, Barros V, Carril A (2004) Differences in El Niño response over the Southern Hemisphere. J Climate 17:1741–1753

Vivier F, Provost C, Meredith MP (2001) Remote and local forcing in the Brazil-Malvinas region. J Phys Oceanogr 31(4):892–913

Wainer I, Venegas S (2002) South Atlantic variability in the climate system model. J Climate 15:1408–1420

Witter DL, Gordon AL (1999) Interannual variability of South Atlantic circulation from 4 years of TOPEX/POSEIDON satellite altimeter observations. J Geophys Res 104(C9):20,927–20,948

Xie S-P (2004) Satellite observations of cool ocean-atmosphere interaction. BAMS 195–208

Zhang R, Rothstein LM, Busalacchi AJ (1998) Origin of upper-ocean warming El Niño change on scales in the Tropical Pacific. Nature 391:879–882

Zhu J, Huang B, Wu Z (2012) The role of ocean dynamics in the interaction between the Atlantic meridional and equatorial modes. J Climate 25(10):3583–3598